International Journal of Minerals, Metallurgy and Materials
Volume 24, Number 2, February 2017, Page 123
DOI: 10.1007/s12613-017-1386-5

Formation and characterization of metallic iron grains in coal-based reduction of oolitic iron ore

Yong-sheng Sun, Yue-xin Han, Yan-feng Li, and Yan-jun Li

School of Resources and Civil Engineering, Northeastern University, Shenyang 110819, China
(Received: 13 May 2016; revised: 23 June 2016; accepted: 6 July 2016)

Abstract: To reveal the formation and characteristics of metallic iron grains in coal-based reduction, oolitic iron ore was isothermally reduced in various reduction times at various reduction temperatures. The microstructure and size of the metallic iron phase were investigated by scanning electron microscopy, energy-dispersive X-ray spectroscopy, and a Bgrimm process mineralogy analyzer. In the results, the reduced Fe separates from the ore and forms metallic iron protuberances, and then the subsequent reduced Fe diffuses to the protuberances and grows into metallic iron grains. Most of the metallic iron grains exist in the quasi-spherical shape and inlaid in the slag matrix. The cumulative frequency of metallic iron grain size is markedly influenced by both reduction time and temperature. With increasing reduction temperature and time, the grain size of metallic iron obviously increases. According to the classical grain growth equation, the growth kinetic parameters, i.e., time exponent, growth activation energy, and pre-exponential constant, are estimated to be 1.3759 ± 0.0374, 103.18 kJ·mol^{-1}, and 922.05, respectively. Using these calculated parameters, a growth model is established to describe the growth behavior of metallic iron grains.

Keywords: iron ore reduction; metallic iron; grain size; growth kinetics; activation energy

1. Introduction

Oolitic iron ore, which widely distributes in Pakistan, France, the United States, the United Kingdom, Canada, and China, is an important iron ore resource [1–3]. Regarded as one of the most refractory iron ores, however, it cannot be upgraded by conventional mineral processing methods because of its unique oolitic texture, complex mineral composition, and high phosphorus content [4–6]. Recently, the coal-based reduction followed by magnetic separation has been provided as a feasible method of recovering iron from refractory iron ores, especially for oolitic iron ore [3,7–10]. In this process, iron minerals are reduced to metallic iron by coal and the metallic iron subsequently grows into the metallic phase with a certain size. Metallic iron that can be used in steel making is then concentrated by magnetic separation after being ground to liberation size.

Numerous excellent works have been conducted on the coal-based reduction of oolitic iron ore. The effects of reduction conditions such as reduction temperature, reduction time, C/O molar ratio, particle size, and coal type on the reduction and magnetic separation were investigated in detail, and metallic iron containing more than 90% Fe was obtained under the optimal conditions [2–3,11–13]. During the reduction, phosphorus was reduced from apatite and partially enriched in the metallic phase, which resulted in the excessive phosphorus content in the metallic iron. Therefore, the additives such as $Ca(OH)_2$, Na_2CO_3, CaO, and Na_2SO_4 were used as the dephosphorization agents to reduce the phosphorus content of the metallic iron, and the satisfactory results were obtained [14–16]. In addition, the distribution behavior and migration mechanism of phosphorus were observed [17–20]. The particle size of metallic iron plays an important role in coal-based reduction and the subsequent magnetic separation, because the metallic iron with large particle size can be easily liberated and separated from the slag. In our previous work, the optical image analysis was used to measure the particle size of metallic iron in reduced oolitic iron ore, and the particle size distribution behavior was analyzed [21–23]. However, the formation and charac-

Corresponding author: Yong-sheng Sun E-mail: yongshengsun@mail.neu.edu.cn
© University of Science and Technology Beijing and Springer-Verlag Berlin Heidelberg 2017

terization of metallic iron grains during the reduction remain unclear, which are imperative for understanding and optimizing the coal-based reduction process.

To obtain the insights into the characteristics of metallic iron during the reduction of oolitic iron ore, the formation process and morphological characterization of metallic iron grains were investigated visually using scanning electron microscopy (SEM) and energy-dispersive X-ray spectroscopy (EDS). The size of the metallic iron grains in reduced iron ore was obtained using a Bgrimm process mineralogy analyzer (BPMA), and the growth kinetics was analyzed on the basis of the classical phenomenological kinetic theory.

2. Experimental procedure

The raw materials used in this research were oolitic iron ore and coal. The oolitic iron ore was collected from Hubei Province, China. Chemical analysis indicated that the main compositions of the ore sample were 42.21wt% Fe, 21.80wt% SiO_2, 5.47wt% Al_2O_3, 4.33wt% CaO, and 1.31wt% P. The microstructure of the ore sample is shown in Fig. 1, which shows that the hematite and chamosite are closely intergrown, forming the typical texture of concentric and alternating layers. The coal used as a reductant was obtained from Jilin Province, China. The proximate analysis results showed that the coal contained 67.83wt% fixed carbon, 18.45wt% volatiles, 12.14wt% ash, and 1.58wt% moisture.

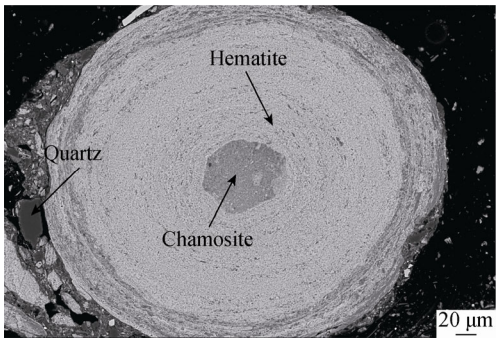

Fig. 1. Microstructure of the ooloitic iron ore sample.

The iron ore and coal were crushed to 100% passing 2 mm and were subsequently mixed according to a mass ratio of 72:28 (iron ore : coal) for use in the reduction experiments. A 100 g sample of the mixture was placed in alumina crucible and isothermally reduced in a muffle furnace under the designated experimental conditions. The reduced samples were then removed and cooled to room temperature in water. After cooling, the reduced samples were characterized by various techniques.

To reveal the formation process of metallic iron grains, the oolitic iron ore was reduced at 1473 K for 2.5, 5, and 7.5 min. The reduced samples were directly characterized by SEM in conjunction with EDS. To quantitatively examine the metallic iron growth, the grain size of metallic iron was measured. The reduced samples were prepared at 1423, 1473, and 1523 K for durations of 20, 30, 40, and 50 min. The SEM images containing more than 1000 metallic iron grains for each specimen were collected from the polished reduced iron ore, and the apparent grain size was subsequently determined by BPMA.

3. Results and discussion

3.1. Formation of metallic iron grains

The iron ore and reduced samples were observed by SEM and EDS, and the results are shown in Fig. 2. As shown in Fig. 2(a), the surface of the oolitic iron ore is relatively smooth. O, Fe, and Si distribute uniformly in the observed region, indicating that O, Fe, and Si are integrated closely with each other in the unreduced oolitic iron.

At the reduction time of 2.5 min, the protuberances and fragmental matter are clearly observed in the reduced ore, as shown in Fig. 2(b). According to the EDS analyses, the protuberances are mainly composed of Fe, whereas the region between protuberances contains Fe, Si, Al, and O. The fragmental matter is iron suboxide formed via the reduction reaction. Fe exhibits the trend of distributing intensively in the protuberance regions. These observations indicate that the protuberances are reduced metallic iron and that the gap regions are a slag matrix phase of Fe–Si–Al–O. After the reduction for 5 min, the protuberances in the reduced ore tend to form spherical-like grains and the amount of fragmental matter obviously increases (Fig. 2(c)). The EDS spectrum of point 7 shows that the protuberance grain is metallic iron and that the purity is higher than that reduced for 2.5 min. Compared with the EDS spectrum of point 6, the relative intensity of the Fe peak weakens significantly, while the intensities of the Al and Si peaks strengthen, indicating the iron oxides in the slag phase are reduced to metallic iron that migrate to the protuberance grains. The distribution regions of Fe, O, and Si are evident. Fe distributes intensively in the protuberance grain regions, whereas Si and O are scattered in the gap regions of protuberance grains. As shown in Fig. 2(d), at a reduction time of 7.5 min, the metallic iron exists in the form of spherical-like grains inlaid in the slag phase. The relative intensity of the O peak in the EDS spectrum of point 12 is weaker than that in point 8, indicating that iron suboxide is further reduced to metallic iron. The distribution of Fe is much more intensive and accurately distributes in the metallic iron grain positions.

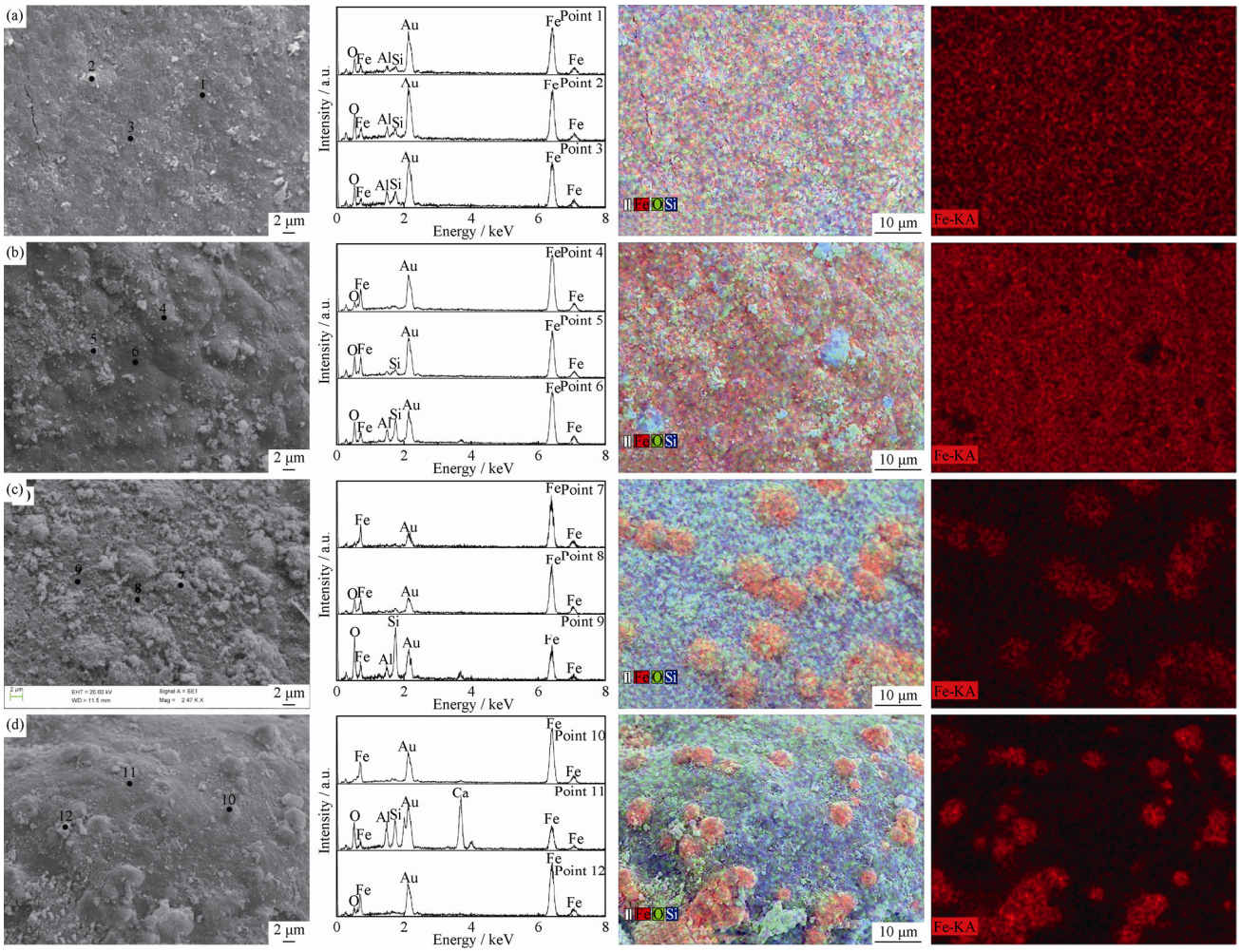

Fig. 2. SEM images and EDS analysis results of the oolitic iron ore reduced at 1473 K: (a) 0 min; (b) 2.5 min; (c) 5 min; (d) 7.5 min.

On the basis of the aforementioned analysis, the formation process of metallic iron grains could be inferred as follows: the iron minerals in the ore surface were firstly reduced to metallic iron atoms that were in a supersaturated state in ore, whereupon the nuclei of metallic iron formed; the new nuclei aggregated with each other via collision and diffusion; the interfacial tension existed in the aggregation process, therefore, the aggregated nuclei separated out from the ore surface and formed tiny metallic iron protuberances; as the reduction proceeded, the iron minerals were further reduced to Fe, and the Fe diffused to the metallic iron protuberances under the action of homogeneous condensation; the metallic iron protuberances then grew into spherical-like grains according to the principle of minimum free energy.

3.2. Characterization of metallic iron grains

As previously mentioned, the metallic iron formed spherical-like particles during the reduction. To obtain the additional details, the iron ore was reduced at 1523 K for 20 min and the reduced sample before and after polished was observed by SEM. The morphology of the metallic iron phase in the reduced iron ore is shown in Fig. 3. As shown in Fig. 3(a), most of the metallic iron phase exhibits a spherical shape and is inlaid in the slag phase that is mainly composed of Si, Al, Ca, Fe, and O. The image of the polished sample (Fig. 3(b)) shows that the metallic iron phase is closely embedded in the slag, and the cross-sectional shape of the metallic iron phase is predominantly round or oval. Therefore, it can be considered that the metallic iron in the reduced ore exists in the form of spherical-like grains.

For a quantitative description, the apparent grain size of metallic iron prepared under different reduction conditions was measured. For a sphere, the real size of metallic iron grain can be calculated according to the following equation [24].

$$d = \frac{4}{\pi} L \tag{1}$$

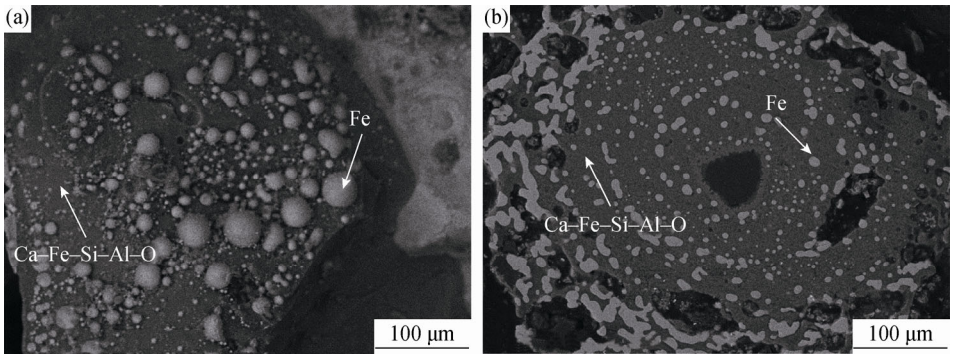

Fig. 3. SEM images of the unpolished (a) and polished (b) samples reduced at 1523 K for 20 min.

where d is the real size and L is the apparent size. The grain size characterization is often expressed as the cumulative distribution of particle properties (e.g., the number, volume, and mass of particles). In this study, the cumulative frequency distribution of metallic iron grains was calculated using the following equation.

$$Q(d) = \frac{n(d < d_i)}{N} \times 100\% \tag{2}$$

where $Q(d)$ is the cumulative frequency, $n(d < d_i)$ the number of metallic iron grains with size smaller than d_i, d_i the measured grain size, and N the total number of measured grains.

The cumulative frequency distribution of metallic iron grains in the reduced samples is shown in Fig. 4. It is observed that the plots of cumulative frequency vs. particle size are quite similar for different reduction conditions. The cumulative frequency obviously increases with increasing particle size, especially when the particle size is small. It is also found that the reduction time and temperature strongly influence the cumulative frequency distribution. At the same reduction temperature, the curves of cumulative frequency shift rightward systematically with increasing reduction time, indicating that the number of large-sized metallic iron grains increases with increasing reduction time. For instance, the D_{80} of metallic iron grains at a reduction temperature of 1473 K increases from 8.97 μm to 30.92 μm as the reduction time is increased from 20 min to 50 min. Similarly, at the same reduction time, the curves of cumulative frequency shift to the right successively with increasing reduction temperature, implying that the number of large metallic iron grains increases. For example, when the reduction temperature increases from 1423 K to 1523 K, the D_{80} at a reduction time of 30 min increases from 10.82 μm to 20.84 μm. These phenomena were attributed to that the increase of reduction time and temperature could accelerate the growth of metallic iron grains, and more large grains were formed under higher temperatures or longer reduction times.

3.3. Growth kinetics of metallic iron grains

To reveal the growth behavior of metallic iron grains, the mean size was used in this study, and it was calculated according to the following equation.

$$\bar{d} = \frac{\sum_{i=1}^{N} d_i}{N} \tag{3}$$

where d is the mean size, d_i the size of each measured metallic iron grain, and N the total number of measured metallic iron grains. The mean size of metallic iron grains at various temperatures for different times is shown in Fig. 5. The grain size of metallic iron obviously increases with the increasing reduction time and temperature. For instance, when the reduction time at 1423 K is increased from 20 min to 50 min, the grain size of metallic iron increases from 4.56 μm to 16.40 μm. This result indicates that the metallic iron gradually grows into large-sized grains with the increasing reduction time and temperature.

Grain growth is usually expressed by the following classical phenomenological kinetic equation [25–29].

$$D^{1/n} - D_0^{1/n} = K \cdot t \tag{4}$$

where D is the grain size, D_0 the grain size at $t = 0$, n the time exponent, K the temperature-dependent growth constant, and t the holding time. The parameter K obeys the Arrhenius relationship.

$$K = K_0 \exp\left(-\frac{Q}{RT}\right) \tag{5}$$

where K_0 is the pre-exponential constant, Q the grain growth activation energy, R the gas constant, and T the absolute temperature. Eq. (4) has been widely used to describe grain growth kinetics during the synthesis of alloys, ceramics, and metals. The growth of the metallic iron phase is regarded as crystal growth. Thus, the metallic iron grain growth is analyzed using this equation. No metallic iron phase is present during the initiation of reduction; thus, D_0 is 0. By substituting

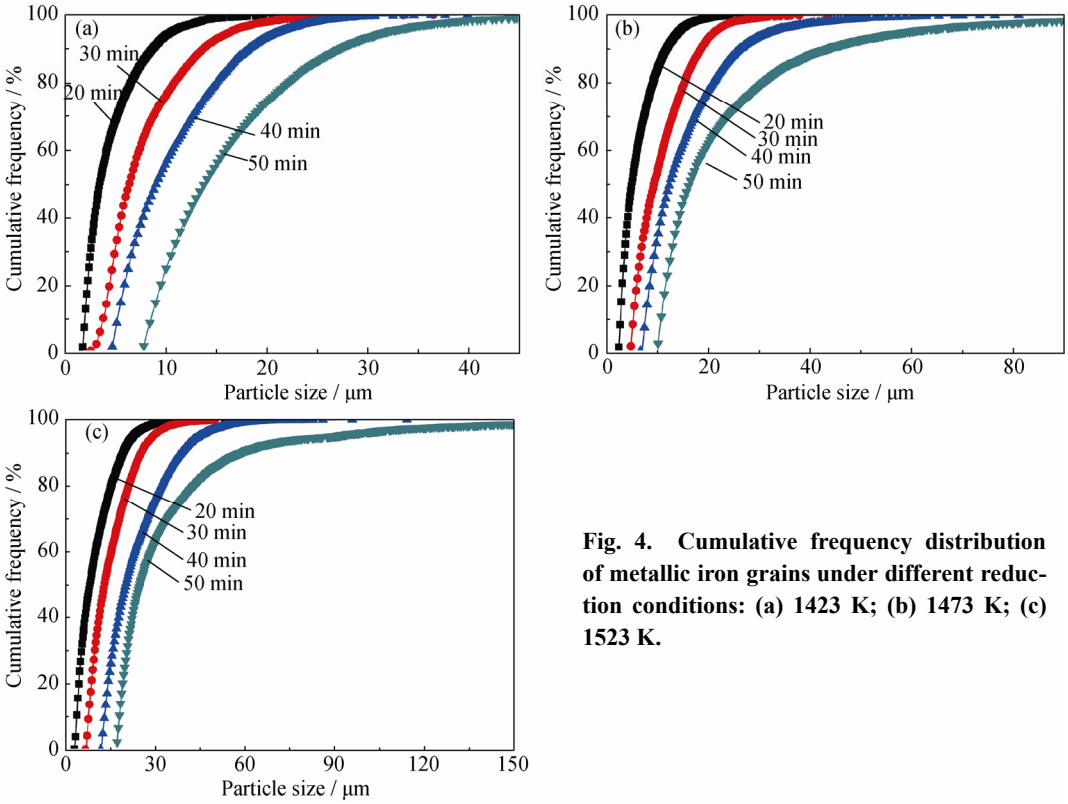

Fig. 4. Cumulative frequency distribution of metallic iron grains under different reduction conditions: (a) 1423 K; (b) 1473 K; (c) 1523 K.

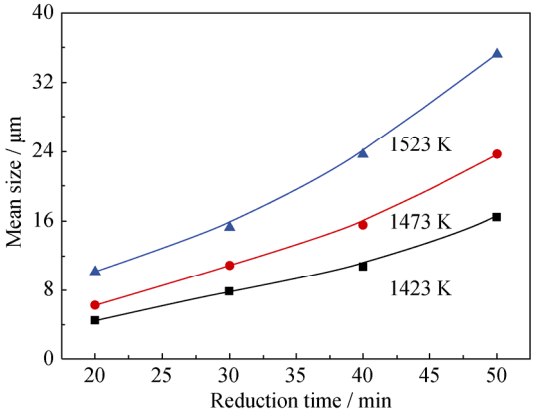

Fig. 5. Mean size of metallic iron grains under different reduction conditions.

Eq. (5) into Eq. (4), the growth of metallic iron grains in the coal-based reduction of the oolitic iron ore can be expressed using the following equation.

$$D^{1/n} = K_0 \exp\left(-\frac{Q}{RT}\right)\cdot t \tag{6}$$

Obviously, if the values of n, K_0, and Q are estimated from the experimental data, the growth model of metallic iron grain will be proposed. To obtain the values of n, K_0, and Q, the grain growth kinetics was analyzed through three successive processes. First, the n value was determined on the basis of the slope of a plot of ln$D$ vs. ln$t$. Second, the K value was obtained from the slope of a plot of $D^{1/n}$ vs. t. Finally, the Q and K_0 values were determined according to the slope and intercept of a plot of ln$K$ vs. $1/T$, respectively.

The plots of ln$D$ vs. ln$t$ are presented in Fig. 6. The linear regression analysis for ln$D$ vs. ln$t$ exhibits good linearity. The n values at different reduction temperatures could be reasonably considered as a constant, 1.3759 ± 0.0374, irrespectively of temperature. The calculation of the grain growth activation energy (Q) and the pre-exponential constant (K_0) is shown in Fig. 7. As presented in Fig. 7(a), the linearity between $D^{1/n}$ ($n = 1.3759 \pm 0.0374$) and t is favorable at various temperatures, and the corresponding K values are

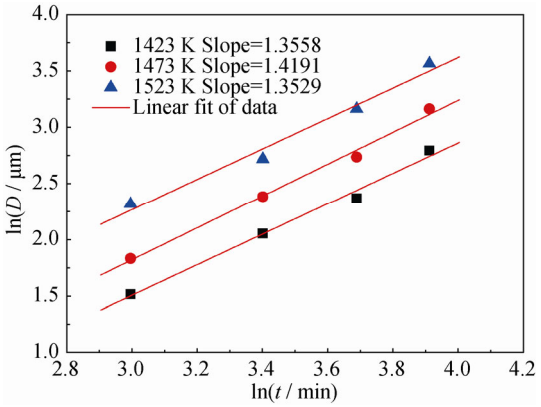

Fig. 6. Plot of ln$D$ vs. ln$t$ for metallic iron grains at different temperatures.

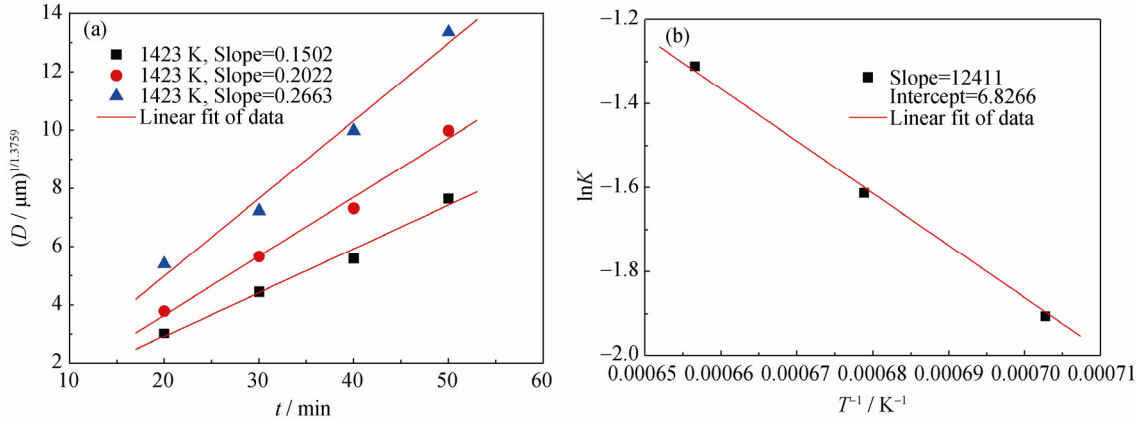

Fig. 7. Determination of Q and K_0 for the growth of metallic iron grains: (a) $D^{1/1.3759}$ vs. t; (b) ln$K$ vs. 1/T.

obtained from the slope regression lines. The dependence of ln$K$ on 1/T is shown in Fig. 7(b). Good linearity is observed between ln$K$ and 1/T. According to the slope and intercept of the regression line, the determined Q and K_0 are 103.18 kJ·mol^{-1} and 922.05, respectively. Using the estimated time exponent, growth activation energy, pre-exponential constant, and Eq. (6), the growth model of metallic iron grains in the coal-based reduction of the oolitic iron ore is derived as

$$D^{1/1.3759} = 922.05 \cdot \exp\left(-\frac{103.18\times10^3}{RT}\right)\cdot t \quad (7)$$

A comparison of the grain sizes calculated using Eq. (7) with experimental data is shown in Fig. 8. The calculated grain sizes are uniformly distributed on the both sides of the equality line, indicating the reasonable agreement between calculations and experimental measurements. Therefore, the established growth model can be used to describe the grain growth of metallic iron in the coal-based reduction of the oolitic iron ore.

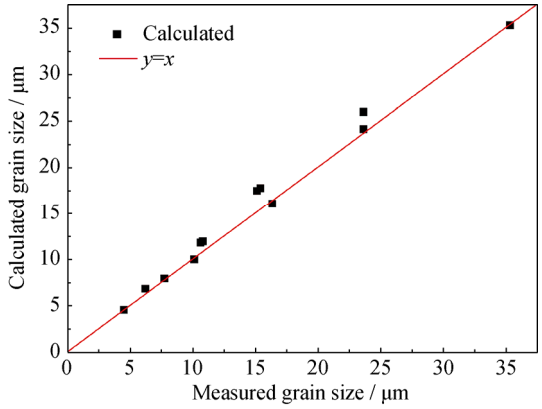

Fig. 8. Reliability of the proposed growth model for metallic iron grains.

4. Conclusions

(1) Iron minerals in the ore surface are first reduced to iron atoms that form metallic iron nuclei. Then the nuclei separate from the ore surface and form tiny metallic iron protuberances as a result of collisions and interfacial tension. Subsequent generated Fe diffuses to the protuberances and grows into spherical-like grains under the action of the minimum free energy principle. Most of the metallic grains exist in the quasi-spherical shape and are closely embedded in the Si–Al–Ca–Fe–O slag phase.

(2) The variation trend of cumulative frequency of metallic iron grain size vs. particle size is approximately the same (obviously increases with the increase of particle size). Both reduction time and temperature strongly influence the growth of metallic iron grains. The curves of cumulative frequency vs. particle size shift toward the right with increasing reduction time and temperature. The mean size of metallic iron grains increases with increasing reduction time and temperature.

(3) The time exponent is almost constant at various temperatures, and the value is 1.3759±0.0374. The growth activation energy and pre-exponential constant for the growth of metallic iron grains is 103.18 kJ·mol^{-1} and 922.05, respectively. The growth kinetics model of metallic iron during coal-based reduction of the oolitic iron ore is described as

$$D^{1/1.3759} = 922.05 \cdot \exp\left(-\frac{103.18\times10^3}{RT}\right)\cdot t \quad \text{for } 1423\ \text{K} \le T \le 1523\ \text{K and } 20\ \text{min} \le t \le 50\ \text{min}$$

where D denotes the size of the metallic iron phase at the reduction time (t) and temperature (T).

Acknowledgements

This work was financially supported by the National Natural Science Foundation of China (Nos. 51134002 and 51604063) and the Fundamental Research Funds for the Central Universities (No. N140108001).

References

[1] S.X. Song, E.F. Campos-Toro, Y.M. Zhang, and A. Lopez-Valdivieso, Morphological and mineralogical characterizations of oolitic iron ore in the Exi region, China, *Int. J. Miner. Metall. Mater.*, 20(2013), No. 2, p. 113.

[2] W. Yu, T.C. Sun, Q. Cui, C.Y. Xu, and J. Kou, Effect of coal type on the reduction and magnetic separation of a high-phosphorus oolitic hematite ore, *ISIJ Int.*, 55(2015), No. 3, p. 536.

[3] Y.S. Sun, Y.X. Han, P. Gao, Z.H. Wang, and D.Z. Ren, Recovery of iron from high phosphorus oolitic iron ore using coal-based reduction followed by magnetic separation, *Int. J. Miner. Metall. Mater.*, 20(2013), No. 5, p. 411.

[4] M.J. Rao, C.Z. Ouyang, G.H. Li, S.H. Zhang, Y.B. Zhang, and T. Jiang, Behavior of phosphorus during the carbothermic reduction of phosphorus-rich oolitic hematite ore in the presence of Na_2SO_4, *Int. J. Miner. Process.*, 143(2015), p. 72.

[5] H.Q. Tang, T.F. Qi, and Y.Q. Qin, Production of low-phosphorus molten iron from high-phosphorus oolitic hematite using biomass char, *JOM*, 67(2015), No. 9, p. 1956.

[6] J.T. Gao, L. Guo, and Z.C. Guo, Concentrating of iron, slag and apatite phases from high phosphorous iron ore gaseous reduction product at 1473 K by super gravity, *ISIJ Int.*, 55(2015), No. 12, p. 2535.

[7] W. Yu, T.C. Sun, Z.Z. Liu, J. Kou, and C.Y. Xu, Study on the strength of cold-bonded high-phosphorus oolitic hematite–coal composite briquettes, *Int. J. Miner. Metall. Mater.*, 21(2014), No. 5, p. 423.

[8] J. Kou, T. Sun, D. Tao, Y. Cao, and C. Xu, Coal-based direct reduction and magnetic separation of lump hematite ore, *Miner. Metall. Process.*, 31(2014), No. 3, p. 150.

[9] T.J. Chun, H.M. Long, and J.X. Li, Alumina–iron separation of high alumina iron ore by carbothermic reduction and magnetic separation, *Sep. Sci. Technol.*, 50(2015), No. 5, p. 760.

[10] U. Srivastava and S.K. Kawatra, Strategies for processing low-grade iron ore minerals, *Miner. Process. Extr. Metall. Rev.*, 30(2009), No. 4, p. 361.

[11] K.Q. Li, W. Ni, M. Zhu, M.J. Zheng, and Y. Li, Iron extraction from oolitic iron ore by a deep reduction process, *J. Iron Steel Res. Int.*, 18(2011), No. 8, p. 9.

[12] S.F. Li, Y.S. Sun, Y.X. Han, G.Q. Shi, and P. Gao, Fundamental research in utilization of an oolitic hematite by deep reduction, *Adv. Mater. Res.*, 158(2011), p. 106.

[13] W. Yu, T.C. Sun, Z.Z. Liu, J. Kou, and C.Y. Xu, Effects of particle sizes of iron ore and coal on the strength and reduction of high phosphorus oolitic hematite-coal composite briquettes, *ISIJ Int.*, 54(2014), No. 1, p. 56.

[14] G.H. Li, S.H. Zhang, M.J. Rao, Y.B. Zhang, and T. Jiang, Effects of sodium salts on reduction roasting and Fe-P separation of high-phosphorus oolitic hematite ore, *Int. J. Miner. Process.*, 124(2013), p. 26.

[15] W. Yu, T.C. Sun, J. Kou, Y.X. Wei, C.Y. Xu, and Z.Z. Liu, The function of $Ca(OH)_2$ and Na_2CO_3 as additive on the reduction of high-phosphorus oolitic hematite-coal mixed pellets, *ISIJ Int.*, 53(2013), No. 3, p. 427.

[16] C.Y. Xu, T.C. Sun, J. Kou, Y. Li, X. Mo, and L.G. Tang, Mechanism of phosphorus removal in beneficiation of high phosphorous oolitic hematite by direct reduction roasting with dephosphorization agent, *Trans. Nonferrous Met. Soc. China*, 22(2012), No. 11, p. 2806.

[17] Y.S. Sun, Y.X. Han, P. Gao, and D.Z. Ren, Distribution behavior of phosphorus in the coal-based reduction of high-phosphorus-content oolitic iron ore, *Int. J. Miner. Metall. Mater.*, 21(2014), No. 4, p. 331.

[18] G.H. Li, M.J. Rao, C.Z. Ouyang, S.H. Zhang, Z.W. Peng, and T. Jiang, Distribution characteristics of phosphorus in the metallic iron during solid-state reductive roasting of oolitic hematite ore, *ISIJ Int.*, (2015), No. 1, p. 1.

[19] C. Cheng, Q.G. Xue, Y.Y. Zhang, F. Han, and J.S. Wang, Dynamic migration process and mechanism of phosphorus permeating into metallic iron with carburizing in coal-based direct reduction, *ISIJ Int.*, 55(2015), No. 12, p. 2576.

[20] J.W. Cha, D.Y. Kim, and S.M. Jung, Distribution behavior of phosphorus and metallization of iron oxide in carbothermic reduction of high-phosphorus iron ore, *Metall. Mater. Trans. B*, 46(2015), No. 5, p. 2165.

[21] Y.S. Sun, Y.X. Han, P. Gao, and Y.F. Mu, Particle size measurement of metallic iron in reduced materials based on optical image analysis, *Chem. Eng. Technol.*, 37(2014), No. 12, p. 2030.

[22] Y.S. Sun, Y.X. Han, P. Gao, and J.W. Yu, Size distribution behavior of metallic iron particles in coal-based reduction products of an oolitic iron ore, *Miner. Process. Extr. Metall. Rev.*, 36(2015), No. 4, p. 249.

[23] Y.X. Han, Y.S. Sun, P. Gao, Y.J. Li, and Y.F. Mu, Particle size distribution of metallic iron during coal-based reduction of an oolitic iron ore, *Miner. Metall. Process.*, 31(2014), No. 3, p. 169.

[24] F. Chayes, On the bias of grain-size measurements made in thin section, *J. Geol.*, 58(1950), No. 2, p. 156.

[25] H. Hu and B.B. Rath, On the time exponent in isothermal grain growth, *Metall. Trans.*, 1(1970), No. 11, p. 3181.

[26] G.W. Yang, X.J. Sun, Q.L. Yong, Z.D. Li, and X.X. Li, Austenite grain refinement and isothermal growth behavior in a low carbon vanadium microalloyed steel, *J. Iron Steel Res. Int.*, 21(2014), No. 8, p. 757.

[27] S. Uhm, J. Moon, C. Lee, J. Yoon, and B. Lee, Prediction model for the austenite grain size in the coarse grained heat affected zone of Fe–C–Mn steels: Considering the effect of initial grain size on isothermal growth behavior, *ISIJ Int.*, 44(2004), No. 7, p. 1230.

[28] J. Reis and R. Chaim, Densification maps for spark plasma sintering of nanocrystalline MgO ceramics: Particle coarsening and grain growth effects, *Mater. Sci. Eng. A*, 491(2008), No. 1-2, p. 356.

[29] R. Chaim, Densification mechanisms in spark plasma sintering of nanocrystalline ceramics, *Mater. Sci. Eng. A*, 443(2007), No. 1-2, p. 25.